

# Boosting quantum battery performance by structure engineering

Junjie Liu<sup>1</sup> and Dvira Segal<sup>1,2</sup>

<sup>1</sup>*Department of Chemistry and Centre for Quantum Information and Quantum Control,  
University of Toronto, 80 Saint George St., Toronto, Ontario, M5S 3H6, Canada*

<sup>2</sup>*Department of Physics, 60 Saint George St., University of Toronto, Toronto, Ontario, M5S 1A7, Canada*  
(Dated: April 15, 2021)

Quantum coherences, correlations and collective effects can be harnessed to the advantage of quantum batteries. Here, we introduce a feasible structure engineering scheme that is applicable to spin-based open quantum batteries. Our scheme, which builds solely upon a modulation of spin energy gaps, allows engineered quantum batteries to exploit spin-spin correlations for mitigating environment-induced aging. As a result of this advantage, an engineered quantum battery can preserve relatively more energy as compared with its non-engineered counterpart over the course of the storage phase. Particularly, the excess in stored energy is independent of system size. This implies a scale-invariant passive protection strategy, which we demonstrate on an engineered quantum battery with staggered spin energy gaps. Our findings establish structure engineering as a useful route for advancing quantum batteries, and bring new perspectives on efficient quantum battery designs.

*Introduction.*— Devising and realizing quantum batteries (QBs) [1] is a rapidly growing research endeavour, requiring sustained and concerted efforts in quantum thermodynamics, quantum information, statistical mechanics, as well as atomic, molecular and optical physics to succeed. In this respect, numerous theoretical architectures are currently being pursued [2–27] (see Ref. [28] for a recent review). Among them, spin-based QBs [3, 5–7, 10–13, 16, 20–22, 24, 26, 27] represent arguably the most promising route towards applications, since spins can be realized in versatile contexts ranging from cavity/circuit quantum electrodynamics (QED) to solid state physics (see Refs. [29, 30] for reviews). The first experimental demonstration of spin-based QB has been carried out recently [31].

To date, a consensus has been reached that quantum mechanical resources such as entanglement and correlations are crucial for achieving quantum advantage of QBs. However, demonstrations of the quantum advantage of QBs are largely focused on the charging and discharging stages [2, 4–7, 10, 11, 13, 15, 16, 23, 32, 33]. In comparison, obtaining a quantum advantage in the storage stage received less attentions due to the viewpoint that QBs in the storage stage can be treated as closed quantum systems that conserve energy (see, e.g., Ref. [5]). However, it is now recognized that QBs in their storage stage warrant an open-system treatment [8, 9, 16, 19–23, 25] since their ability to store and conserve energy for later purposes is plagued by the unavoidable dissipation stemming from interactions with surrounding environments. Hence, safeguarding open QBs during their storage phase is central to the mission of realizing QBs for quantum technological applications, calling for efforts to exploit non-trivial quantum effects for circumventing this practical challenge.

In this work, we introduce a simple and feasible route for harnessing spin-spin correlations for protecting spin-based QBs during the storage phase. Our proposal relies on a structure engineering (SE) of spin-based QBs by the modulation of spins energy gap, aiming for breaking the translational invariance of the bulk of spin-based QBs. Building on SE, spin-

spin correlations are utilized to impact spin population dynamics, altering its decaying pattern from a fast exponential trend to a slower non-exponential decay. Spin-spin correlations can therefore be harnessed for mitigating aging of spin-based QBs [12], prolonging the storage time of charged QBs. The so-obtained protection strategy expands the family of passive protection protocols in the storage stage [8, 9, 16, 21, 23]. We remark that passive protection strategies are favored from a thermodynamic perspective since their active counterparts (see Refs. [19, 20, 22, 25]) cost extra energy for implementation, thereby reducing the overall efficiency of QBs.

To illustrate the SE strategy, we consider a prototype spin-cavity architecture for spin-based QBs [5, 7, 10, 12, 31]. The working substance consists of a one-dimensional spin-1/2 lattice with uniform nearest-neighbor dipole-dipole coupling strengths. The potential of SE is highlighted by contrasting a dimeric engineered QB with staggered spin energy gaps (see Fig. 1) to a non-engineered model with identical units. Exploiting analytical solutions of quantum Lindblad master

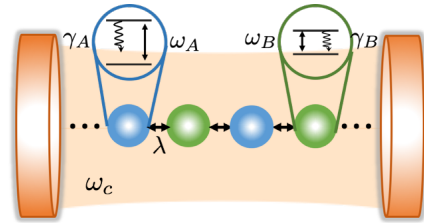


Figure 1. Scheme of a structure-engineered quantum battery architecture consisting a cavity and a working substance—a dimeric spin lattice with staggered energy gaps  $\omega_{A,B}$  and decay rates  $\gamma_{A,B}$ . Nearest-neighbor dipole-dipole couplings  $\lambda$  is assumed uniform. In the storage phase, the dimeric spin lattice is decoupled from the cavity (frequency  $\omega_c$ ), whereas in the charging and discharging phases the light-matter interaction is turned on and the cavity serves as a charger [5, 7, 10, 31] (with possible external driving fields) and a superradiant decay channel for spins [12], respectively.

equation [34] available for the single-excitation sector of the Hilbert space, we confirm the cooperation of spin-spin cor-

relations in spin population dynamics in an engineered QB, leading to a slower spin decaying pattern. On the contrary, spin population dynamics in the non-engineered counterpart exhibits a fast exponential decay trend. From the energetics, quantified by the stored total energy, we further show that an engineered QB significantly outperforms its non-engineered counterpart, with more energy preserved during the storage phase. In particular, we find that the relative energy gain is independent of system size, indicating that we achieved a scale-invariant protection with potential applications to future scalable quantum battery setups.

*Microscopic model.*—We consider a spin-cavity architecture (see Fig. 1 for a sketch) in light of existing theoretical proposals [5, 7, 10, 12], and a recent experimental work [31]. The QB model includes a one-dimensional spin-1/2 lattice as the working substance with spin gaps  $\{\omega_j\}$ , Pauli spin operators  $\{\sigma_j^{z,\pm}\}$  ( $\sigma_j^- = (\sigma_j^+)^{\dagger}$ ),  $j \in [1, \dots, N]$  (setting  $N$  an even number), and nearest-neighbor dipole-dipole interactions measured by the strength  $\lambda$ . The spins are coupled to an optical cavity supporting a single dispersionless mode with frequency  $\omega_c$  and annihilation operator  $a$ . The light-matter coupling, measured by strength  $\eta$ , is treated within the rotating-wave-approximation. In the rotating frame, we obtain the total Hamiltonian (setting  $\hbar = 1$ ),

$$H_{\text{tot}} = \sum_{j=1}^N \frac{\Delta_j}{2} \sigma_j^z + \sum_{j=1}^{N-1} \lambda (\sigma_j^+ \sigma_{j+1}^- + \text{H.c.}) + \eta \sum_{j=1}^N (\sigma_j^- a^{\dagger} + \text{H.c.}). \quad (1)$$

Here,  $\Delta_j = \omega_j - \omega_c$ , ‘H.c.’ is short for ‘Hermitian conjugate’. Our results in the storage phase do not depend on the frequency  $\omega_c$  itself.

In addition to the coherent Hamiltonian  $H_{\text{tot}}$ , incoherent processes affect the QB. These include the decay of the intensity of the field within the cavity, with a rate constant  $\kappa$ , and the spontaneous decay of spins, with rate constants  $\gamma_j$ . In the weak dissipation regime of  $\gamma_j \ll \Delta_j$ ,  $\kappa \ll \omega_c$ , the total density matrix  $\rho_{\text{tot}}$  of the cavity and spins is governed by the following Lindblad master equation [34] (explicit time dependence is suppressed)

$$\frac{\partial}{\partial t} \rho_{\text{tot}} = -i[H_{\text{tot}}, \rho_{\text{tot}}] + \kappa \mathcal{L}[a] \rho_{\text{tot}} + \sum_{j=1}^N \gamma_j \mathcal{L}[\sigma_j^-] \rho_{\text{tot}}. \quad (2)$$

Here,  $\mathcal{L}[O] \rho_{\text{tot}} = (2O \rho_{\text{tot}} O^{\dagger} - O^{\dagger} O \rho_{\text{tot}} - \rho_{\text{tot}} O^{\dagger} O)/2$  denotes the Lindblad superoperator. We neglect dephasing and heating (incoherent pumping) of spins, as their rates can be made several orders of magnitude smaller than individual decay rates [35].

We limit our analysis to the storage phase. Following Ref. [12] we assume that the QB is fully charged (through the cavity [5, 7, 10]) at time  $t = 0$  when the storage stage begins. During the storage stage we turn off the light-matter interaction by tuning the cavity frequency away from  $\omega_j$ . Hence, in the storage stage we just consider the reduced quantum master equation for spins (see the supplemental material [36] for

more details),

$$\frac{\partial}{\partial t} \rho_S = -i[H_S, \rho_S] + \sum_{j=1}^N \gamma_j \mathcal{L}[\sigma_j^-] \rho_S \equiv \mathbb{L} \rho_S. \quad (3)$$

Here,  $H_S = \sum_{j=1}^N \frac{\Delta_j}{2} \sigma_j^z + \sum_{j=1}^{N-1} \lambda (\sigma_j^+ \sigma_{j+1}^- + \sigma_{j+1}^+ \sigma_j^-)$  is the spin lattice Hamiltonian in the rotating frame,  $\mathbb{L}$  is the total Liouvillian.

*Structure engineering scheme.*—We begin with dynamical equations for spin population  $\langle \sigma_z^j \rangle$  obtained using Eq. (3),

$$\begin{aligned} \frac{d}{dt} \langle \sigma_z^j \rangle = & -2i\lambda \left[ \langle \sigma_j^+ \sigma_{j+1}^- \rangle + \langle \sigma_j^+ \sigma_{j-1}^- \rangle - \langle \sigma_{j+1}^+ \sigma_j^- \rangle \right. \\ & \left. - \langle \sigma_{j-1}^+ \sigma_j^- \rangle \right] - \gamma_j \langle 1 + \sigma_j^z \rangle. \end{aligned} \quad (4)$$

For long spin lattices with  $N \gg 1$ , we can neglect boundary effects and focus on the bulk of the QB. We observe that the first four terms, representing spin-spin correlations, cancel out exactly in the bulk of a uniform spin lattice with a translational invariance since, for instance,  $\langle \sigma_{j-1}^+ \sigma_j^- \rangle = \langle \sigma_j^+ \sigma_{j+1}^- \rangle$ . As a result, even though spin-spin correlations are nonzero, the spin population of a uniform spin lattice decays exponentially and locally, in the sense that the decaying dynamics is independent of other spins, leading to an aging of charged QBs [12].

Can one harness spin-spin correlations to mitigate aging? We answer this question affirmatively by introducing a strategy based on SE, building solely on the modulation of spin energy gaps such that, for instance, we should at least have  $\Delta_j \neq \Delta_{j\pm 1}$  in the present model. Through SE, realized here with the addition of non-homogeneity of spin energy gaps to the otherwise uniform lattice, we break the translation invariance of the bulk such that  $\langle \sigma_{j-1}^+ \sigma_j^- \rangle \neq \langle \sigma_j^+ \sigma_{j+1}^- \rangle$ , resulting in nonzero contributions from spin-spin correlations to the spin population dynamics. The result of the inclusion of spin-spin correlations is that we can alter the decaying pattern of spin populations from a fast exponential trend to a non-exponential one. More intriguingly, the SE simultaneously modifies the spontaneous emission rate  $\gamma_j$  as it is proportional to the spin energy gap (see, e.g., Ref. [37]). Hence the engineered decay dynamics can become relatively slower, thereby mitigating aging effect in a passive manner.

Although here we lay out the SE scheme by focusing on a spin lattice with nearest-neighbor couplings, we emphasize that our SE scheme is not limited to this specific case. In fact, SE strategies can be tailored for other spin lattice models by inspecting the detailed form of the dynamical equations governing spin population dynamics, which is model dependent; more discussions will be provided later.

*Dimeric lattice and single-excitation sector.*—To facilitate the analysis with numerical insights, we adopt a dimeric SE: A dimeric spin lattice with staggered energy gaps  $\Delta_{A,B}$  and decay rates  $\gamma_{A,B}$  ( $\gamma_A/\Delta_A = \gamma_B/\Delta_B$ ) but uniform dipole-dipole coupling strength  $\lambda$  (see Fig. 1) [38]. Without loss of generality, we set  $\Delta_j = \Delta_{A(B)}$  if  $j$  is odd (even). We note that a dimeric SE can either speed or slow the decay dynamics of the spin populations, compared to that of the non-engineered lattice ( $\Delta_A = \Delta_B$ ), depending on the ratio  $\Delta_B/\Delta_A$ . For our

purposes, we refer to the system with  $\Delta_A = \Delta_B$  ( $\Delta_A > \Delta_B$ ) as the non-engineered (engineered) QB.

We first focus on the single-excitation sector of the spin Hilbert space containing one spin excitation in total. Notably, the slowest decay dynamics of the system belongs to this sector [39, 40]. Since the jump term  $\sum_j \gamma_j \sigma_j^- \rho_S \sigma_j^+$  of the Lindblad master equation Eq. (3) does not contribute in this sector, the dissipative dynamics is fully governed by the part  $\partial \rho_S / \partial t = \mathcal{K} \rho_S \equiv -i[K \rho_S - \rho_S K^\dagger]$  with an effective (non-Hermitian) Hamiltonian  $K \equiv H_S - i \sum_j \frac{\gamma_j}{2} \sigma_j^+ \sigma_j^-$ . Since  $K$  is quadratic, one easily finds its two-band complex eigenvalues under an open boundary condition [40]  $\Omega_k^\pm = [(\Omega_A + \Omega_B)/2] \pm \frac{1}{2} \sqrt{(\Omega_A - \Omega_B)^2 + 16\lambda^2 \cos^2(k/2)}$ . Here,  $\Omega_{A(B)} = \Delta_{A(B)} - i\gamma_{A(B)}$  and  $k = 2\pi l/(N+1)$  with  $l = 1, 2, \dots, N/2$ . The eigenvalues of  $K^\dagger$  are the complex conjugates  $\Omega_k^{\pm*}$ . In general, the eigenvalues of the Liouvillian  $\mathbb{L}$  can be constructed by using  $\Omega_k^\pm$  and  $\Omega_k^{\pm*}$  as detailed in Ref. [39], while the smallest decay rates are  $-\text{Im}[\Omega_k^\pm]$  with ‘Im’ taking imaginary part. For a uniform lattice with  $\Omega_A = \Omega_B$ , we have  $-\text{Im}[\Omega_k^\pm] = \gamma_A$ . Notably, the inverse of  $\gamma_A$  sets the storage timescale for the non-engineered QB [12]. On the contrary, we find that the smallest decay rates of the dimeric spin lattice is smaller than that of the uniform lattice (see the supplemental material [36]), indicating a longer storage time.

To quantify the dynamical behavior, we study spin populations  $\langle \sigma_j^z(t) \rangle$  and spin-spin correlations  $\langle \sigma_j^+(t) \sigma_{j'}^-(t) \rangle$ , which have the following analytical expressions in the single-excitation sector [40],

$$\begin{aligned} \langle \sigma_j^z(t) \rangle &= 2 \sum_{n,m} G_{n,m}(j) e^{-i(\Omega_n - \Omega_m^*)t} - 1, \\ \langle \sigma_j^+(t) \sigma_{j'}^-(t) \rangle &= \sum_{n,m} W_{n,m}(j, j') e^{-i(\Omega_n - \Omega_m^*)t}. \end{aligned} \quad (5)$$

Here,  $\Omega_n$  with  $n$  running from 1 to  $N$  are elements of a  $1 \times N$  vector  $\mathbf{\Omega}$  whose first (second) half belongs to  $\Omega_k^-$  ( $\Omega_k^+$ ) with  $k$  running from  $2\pi/(N+1)$  to  $\pi N/(N+1)$  (see above). The coefficients  $G_{n,m}(j)$  and  $W_{n,m}(j, j')$  are determined by the eigenvectors of  $K$  and  $K^\dagger$ , as well as by the initial condition  $\rho_S(0)$ ; we relegate their detailed expressions to the supplemental material [36].

In Fig. 2, we present results for population  $\langle \sigma_j^z(t) \rangle$  and spin-spin correlation  $\langle \sigma_j^+(t) \sigma_{j'}^-(t) \rangle$  at the bulk of the spin chain (sites  $j = 10$  and  $j = 11$ ). We use Eq. (5) and assume the (arbitrary) initial state  $\rho_S(0) = |\Phi_0\rangle\langle\Phi_0|$ ;  $|\Phi_0\rangle = |g\rangle/\sqrt{2} + (|e_{j=10}\rangle + |e_{j=12}\rangle)/2$  with  $|e_j\rangle = \sigma_j^+|g\rangle$  and  $|g\rangle$  the global ground state of the spins, namely,  $\sigma_j^z|g\rangle = -|g\rangle$ . We confirmed that basic features depicted in Fig. 2 are independent of the initial condition adopted in the single-excitation sector. From Fig. 2 (a), it is evident that spin population in a uniform (non-engineered) lattice (dash-dotted line) decays initially in an exponential manner. In comparison, the spin population in a dimeric lattice (solid line) depicts a slower decay, dressed by an oscillatory behavior at short times. Moreover, by the time  $\Delta_A t = 25$ , the excited state population in the uniform case is close to zero, while in the dimerized case by that time only 40% had decayed to the ground state.

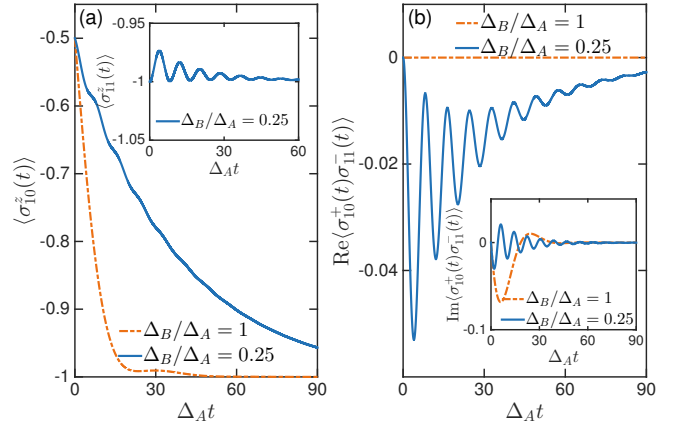


Figure 2. (a) Trajectory of  $\langle \sigma_{10}^z(t) \rangle$  in a single-excitation sector using Eq. (5) for  $\Delta_B/\Delta_A = 0.25$  (blue solid line) and  $\Delta_B/\Delta_A = 1$  (orange dash-dotted line). Inset: Trajectory of  $\langle \sigma_{11}^z(t) \rangle$  for  $\Delta_B/\Delta_A = 0.25$ . (b) Trajectory of the real (Re) part of the spin-spin correlation  $\langle \sigma_{10}^+(t) \sigma_{11}^-(t) \rangle$  using Eq. (5) for  $\Delta_B/\Delta_A = 0.25$  (blue solid line) and  $\Delta_B/\Delta_A = 1$  (orange dash-dotted line). Inset: Trajectory of the imaginary (Im) part of the spin-spin correlation  $\langle \sigma_{10}^+(t) \sigma_{11}^-(t) \rangle$ . Other parameters are  $N = 50$ ,  $\gamma_{A,B}/\Delta_{A,B} = 0.05$ ,  $\lambda = 0.05\Delta_A$ .

Based on the SE scheme and Eq. (4), we naturally expect that transient oscillations of the spin population (see also the inset for a nearest-neighbor site) in the dimeric lattice arise from the spin-spin correlations. To verify whether this is the case, we turn to the spin-spin correlation result showed in Fig. 2 (b). For clarity and simplicity, we just depict  $\langle \sigma_{10}^+(t) \sigma_{11}^-(t) \rangle$  in accordance with population results of Fig. 2 (a). From Fig. 2 (b), we immediately note that spin-spin correlations in the dimeric lattice oscillate with a period that is consistent with that inferred from spin population dynamics at short times, confirming that spin-spin correlations indeed affect spin population dynamics in the dimeric lattice. In comparison, although we have nonzero spin-spin correlations in a uniform lattice, its impact on spin population dynamics is negligible, in accordance with Eq. (4). Hence, from the dynamics in the single-excitation sector, we confirm that SE (i) allows for the participation of spin-spin correlation in spin population dynamics, and (i) leads to slower decaying trend of spin populations, thereby mitigating the aging effect.

*Energetics in the storage phase.*— To characterize the performance of a fully-charged engineered QB, we turn to the energetics in the storage phase. This requires information of higher-order excitation sectors as we have  $N$  excitations at  $t = 0$  ( $\langle \sigma_j^z(t = 0) \rangle = 1$  but spin coherences and correlations are set to zero), namely, the full Lindblad master equation Eq. (3) should be utilized. We consider the dynamics of the average total energy normalized by frequencies,

$$\mathcal{E}(t) \equiv \frac{\langle H_S(t) \rangle}{\sum_{j=1}^N \Delta_j/2}. \quad (6)$$

This measure allows for a proper comparison between engineered and non-engineered QBs. It has been demonstrated for

spin-based QBs that the average total energy approaches the ergotropy—the maximal extractable work under a cyclic unitary transformation [41]—in the large  $N$  limit [10, 16, 21]. We thus perform simulations in this limit. We denote by  $\mathcal{E}_{d(u)}(t)$  the average total energy in the dimeric (uniform) lattice. The dynamics of  $\mathcal{E}(t)$  is obtained by solving Eq. (4) together with those for higher-order correlation terms based on Eq. (3); coupled equations of motion obtained under a second-order cumulant approximation [42, 43] applicable for large  $N$  are listed in the supplemental material [36].

In Fig. 3, we show the dynamics of the relative energy excess  $[\mathcal{E}_d(t) - \mathcal{E}_u(t)]/\mathcal{E}_u(t)$  during the storage phase; a similar comparison for the averaged population is depicted in the supplemental material [36]. We observe several features that are

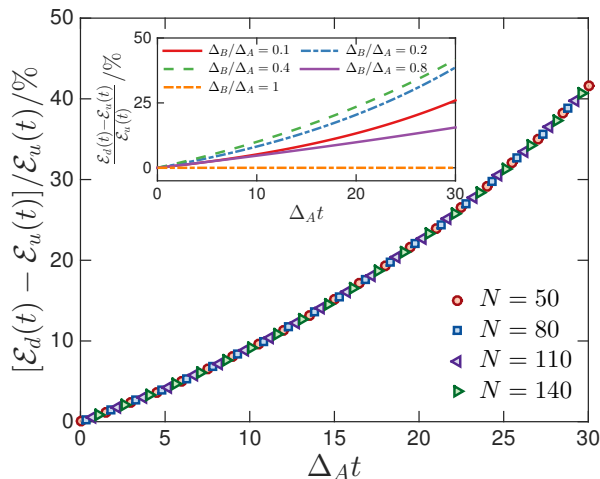


Figure 3. Dynamics of relative stored energy excess  $[\mathcal{E}_d(t) - \mathcal{E}_u(t)]/\mathcal{E}_u(t)$  in the storage phase as a function of spin numbers  $N$  with a fixed detuning ratio  $\Delta_B/\Delta_A = 0.25$ . Inset: Relative excess energy when varying detuning ratio  $\Delta_B/\Delta_A$  at a fixed number  $N = 80$ . Other parameters are  $\gamma_{A(B)}/\Delta_{A(B)} = 0.05$  and  $\lambda = 0.05\Delta_A$ .

worth mentioning: (i) The engineered QB preserves more energy than the non-engineered counterpart as the storage time goes. Particularly, the relative excess  $[\mathcal{E}_d(t) - \mathcal{E}_u(t)]/\mathcal{E}_u(t)$  is monotonic as a function of storage time. Approximately, we reveal the scaling  $\mathcal{E}_d(t)/\mathcal{E}_u(t) \propto t^\alpha$  with  $\alpha = 1.5$  at long times [36]. Notwithstanding, we point out that the absolute excess  $\mathcal{E}_d(t) - \mathcal{E}_u(t)$  shows a turnover behavior when increasing the storage time [36], implying an optimal protection time for the engineered QB. Notably, one can also infer this property from Fig. 2 (a) for the population dynamics in the one-excitation sector, identified by the maximum population contrast appears around  $\Delta_A t \sim 30$ . (ii) The *relative* excess is independent of the number of spins  $N$ , indicating that the resulting passive protection scheme is scale-invariant and can be applied to large-scale QBs. (iii) The inset shows that the relative excess is a nonmonotonic function in the frequency ratio  $\Delta_B/\Delta_A$ , with the maximum achieved at an intermediate value. This property indicates that the so-obtained advantage

of engineered QBs is not merely a consequence of the modification of decay rates from  $\gamma_A$  to  $\gamma_B$  for spins with even indices, otherwise, we should have observed a monotonic dependence of the relative excess on the frequency ratio  $\Delta_B/\Delta_A$  as  $\gamma_B$  monotonically approaches  $\gamma_A$  when we increase the ratio. We note that such a dimeric spin lattice allows for an intriguing collective spin motion, namely, quantum *transient* synchronization [40] as featured by decaying oscillations of spin coherences  $\langle \sigma_j^x(t) \rangle$ , with the same frequency, in spite of distinct intrinsic spin frequencies (see the supplemental material [36] for trajectories with varying  $\Delta_B/\Delta_A$ ). Interestingly, this synchronization only occurs within a specific range of frequency ratio [36, 40]. We therefore argue that the observed nonmonotonic behavior in energy stored indicates that the nontrivial collective spin motion enabled by spin-spin correlations contributes to the advantage of engineered QBs.

*Discussion.*— We envision realization of the engineered QB using circuit QED architectures involving superconducting qubits [29, 30, 44–47], leveraging an exquisite tunability over system parameters such as the qubit frequency. Furthermore, one can easily scale up the system size in circuit QED [48], allowing for scalable QB designs. The implementation of the engineered QB is not tied to circuit QED setups in light of parallel advances in a variety of other experimental platforms, including cold atoms [49–52], quantum dots [53, 54], and trapped ions [55] in optical traps and photonic structures, where spins connected in a one-dimensional arrangement are concerned.

Two possible extensions of the present strategy to more complicated QB designs are anticipated: (i) Many-body QBs with long-range spin-spin couplings beyond nearest-neighbor order [6, 16]. In this scenario, equations of motion for spin populations involve long-range correlation terms and we expect engineered structures beyond a dimeric configuration, depending on the details of the underlying spin-spin interaction pattern. (ii) QBs in higher dimensions. Taking a possible two-dimensional QB as an example, we anticipate that the same approach of SE would directly apply if we limit spin-spin interactions to lowest nearest-neighbor terms. Although experimental techniques for connecting spins in two-dimensional arrangements are mature [56, 57], it is challenging to implement the dimeric lattice as it creates a certain spatial-ordered pattern with two kinds of spins. We defer those ideas to future studies.

In summary, we introduced a generic SE scheme applicable to spin-based QBs, obtained by inspecting the dynamical equations of motion for spin populations [cf. Eq. (4) for a lattice with nearest-neighbor couplings]. Through a modulation of spin energy gap, the engineered QB can harness spin-spin correlations to mitigate aging effect in the storage stage, thereby achieving an advantage in extending the longevity of charged QBs. We expect that the resulting scale-invariant protection strategy, which is applicable in noisy environments, to play a central role in boosting the performance of QBs.

*Acknowledgement.*— We thank Albert Cabot for insightful discussions and assistance in simulations, and Ilia Khaït for

critical reading of the manuscript. This work was supported by the Natural Sciences and Engineering Research Council (NSERC) of Canada Discovery Grant and the Canada Research Chairs Program.

- 
- [1] F. Campaioli, F. A. Pollock, and S. Vinjanampathy, “Quantum batteries,” in *Thermodynamics in the Quantum Regime: Recent Progress and Outlook*, edited by F. Binder, L. A. Correa, C. Gogolin, J. Anders, and G. Adesso (Springer, 2018).
- [2] R. Alicki and M. Fannes, “Entanglement boost for extractable work from ensembles of quantum batteries,” *Phys. Rev. E* **87**, 042123 (2013).
- [3] F. C. Binder, S. Vinjanampathy, K. Modi, and J. Goold, “Quantacell: powerful charging of quantum batteries,” *New J. Phys.* **17**, 075015 (2015).
- [4] F. Campaioli, F. A. Pollock, F. C. Binder, L. Céleri, J. Goold, S. Vinjanampathy, and K. Modi, “Enhancing the charging power of quantum batteries,” *Phys. Rev. Lett.* **118**, 150601 (2017).
- [5] D. Ferraro, M. Campisi, G. M. Andolina, V. Pellegrini, and M. Polini, “High-power collective charging of a solid-state quantum battery,” *Phys. Rev. Lett.* **120**, 117702 (2018).
- [6] T. P. Le, J. Levinsen, K. Modi, M. M. Parish, and F. A. Pollock, “Spin-chain model of a many-body quantum battery,” *Phys. Rev. A* **97**, 022106 (2018).
- [7] G. M. Andolina, D. Farina, A. Mari, V. Pellegrini, V. Giovannetti, and M. Polini, “Charger-mediated energy transfer in exactly solvable models for quantum batteries,” *Phys. Rev. B* **98**, 205423 (2018).
- [8] J. Liu, D. Segal, and G. Hanna, “Loss-free excitonic quantum battery,” *J. Phys. Chem. C* **123**, 18303 (2019).
- [9] A. C. Santos, B. Çakmak, S. Campbell, and N. T. Zinner, “Stable adiabatic quantum batteries,” *Phys. Rev. E* **100**, 032107 (2019).
- [10] G. Andolina, M. Keck, A. Mari, M. Campisi, V. Giovannetti, and M. Polini, “Extractable work, the role of correlations, and asymptotic freedom in quantum batteries,” *Phys. Rev. Lett.* **122**, 047702 (2019).
- [11] Y. Zhang, T. Yang, L. Fu, and X. Wang, “Powerful harmonic charging in a quantum battery,” *Phys. Rev. E* **99**, 052106 (2019).
- [12] F. Pirmoradian and K. Mølmer, “Aging of a quantum battery,” *Phys. Rev. A* **100**, 043833 (2019).
- [13] G. M. Andolina, M. Keck, A. Mari, V. Giovannetti, and M. Polini, “Quantum versus classical many-body batteries,” *Phys. Rev. B* **99**, 205437 (2019).
- [14] D. Farina, G. M. Andolina, A. Mari, M. Polini, and V. Giovannetti, “Charger-mediated energy transfer for quantum batteries: An open-system approach,” *Phys. Rev. B* **99**, 035421 (2019).
- [15] D. Rossini, G. M. Andolina, D. Rosa, M. Carrega, and M. Polini, “Quantum advantage in the charging process of sachdev-ye-kitaev batteries,” *Phys. Rev. Lett.* **125**, 236402 (2020).
- [16] D. Rossini, G. M. Andolina, and M. Polini, “Many-body localized quantum batteries,” *Phys. Rev. B* **100**, 115142 (2019).
- [17] F. Barra, “Dissipative charging of a quantum battery,” *Phys. Rev. Lett.* **122**, 210601 (2019).
- [18] K. V. Hovhannisyanyan, F. Barra, and A. Imparato, “Charging assisted by thermalization,” *Phys. Rev. Research* **2**, 033413 (2020).
- [19] S. Gherardini, F. Campaioli, F. Caruso, and F. C. Binder, “Stabilizing open quantum batteries by sequential measurements,” *Phys. Rev. Research* **2**, 013095 (2020).
- [20] A. C. Santos, A. Saguia, and M. S. Sarandy, “Stable and charge-switchable quantum batteries,” *Phys. Rev. E* **101**, 062114 (2020).
- [21] J. Quach and W. Munro, “Using dark states to charge and stabilize open quantum batteries,” *Phys. Rev. Applied* **14**, 024092 (2020).
- [22] S.-Y. Bai and J.-H. An, “Floquet engineering to reactivate a dissipative quantum battery,” *Phys. Rev. A* **102**, 060201 (2020).
- [23] D. Rosa, D. Rossini, G. M. Andolina, M. Polini, and M. Carrega, “Ultra-stable charging of fast-scrambling sachdev-ye-kitaev quantum batteries,” *J. High Energ. Phys.* **2020**, 67 (2020).
- [24] F. H. Kamin, F. T. Tabesh, S. Salimi, F. Kheirandish, and A. C. Santos, “Non-markovian effects on charging and self-discharging process of quantum batteries,” *New J. Phys.* **22**, 083007 (2020).
- [25] M. T. Mitchison, J. Goold, and J. Prior, “Charging a quantum battery with linear feedback control,” ArXiv:2012.00350.
- [26] S. Ghosh, T. Chanda, and A. Sen(De), “Enhancement in the performance of a quantum battery by ordered and disordered interactions,” *Phys. Rev. A* **101**, 032115 (2020).
- [27] F. Caravelli, G. Coulter-De Wit, L. García-Pintos, and A. Hamma, “Random quantum batteries,” *Phys. Rev. Research* **2**, 023095 (2020).
- [28] S. Bhattacharjee and A. Dutta, “Quantum thermal machines and batteries,” ArXiv:2008.07889.
- [29] A. Blais, S. M. Girvin, and W. D. Oliver, “Quantum information processing and quantum optics with circuit quantum electrodynamics,” *Nat. Phys.* **16**, 247 (2020).
- [30] G. Burkard, M. J. Gullans, X. Mi, and J. R. Petta, “Superconductor-semiconductor hybrid-circuit quantum electrodynamics,” *Nat. Rev. Phys.* **2**, 129 (2020).
- [31] J. Q. Quach, K. E. McGhee, L. Ganzer, D. M. Rouse, B. W. Lovett, E. M. Gauger, J. Keeling, G. Cerullo, D. G. Lidzey, and T. Virgili, “An organic quantum battery,” ArXiv:2012.06026.
- [32] S. Julià-Farré, T. Salamon, A. Riera, M. N. Bera, and M. Lewenstein, “Bounds on the capacity and power of quantum batteries,” *Phys. Rev. Research* **2**, 023113 (2020).
- [33] L. P. García-Pintos, A. Hamma, and A. del Campo, “Fluctuations in extractable work bound the charging power of quantum batteries,” *Phys. Rev. Lett.* **125**, 040601 (2020).
- [34] G. Lindblad, “On the generators of quantum dynamical semigroups,” *Commun. Math. Phys.* **48**, 119 (1976).
- [35] H. Schwager, J. I. Cirac, and G. Giedke, “Dissipative spin chains: Implementation with cold atoms and steady-state properties,” *Phys. Rev. A* **87**, 022110 (2013).
- [36] See Supplemental Material for details related to the dynamics in single-excitation sector, derivations of coupled dynamical equations of motion for spins and additional simulation results.
- [37] P. Lodahl, S. Mahmoodian, and S. Stobbe, “Interfacing single photons and single quantum dots with photonic nanostructures,” *Rev. Mod. Phys.* **87**, 347–400 (2015).
- [38] For systems with nearest-neighbor couplings, we note that a dimeric lattice is sufficient to break the translational invariance. However, one can consider more complicated structural engineering, for instance, a trimeric lattice.
- [39] J. M. Torres, “Closed-form solution of lindblad master equations without gain,” *Phys. Rev. A* **89**, 052133 (2014).
- [40] A. Cabot, G. Giorgi, F. Galve, and R. Zambrini, “Quantum synchronization in dimer atomic lattices,” *Phys. Rev. Lett.* **123**, 023604 (2019).
- [41] A. E. Allahverdyan, R. Balian, and T. M. Nieuwenhuizen,

- “Maximal work extraction from finite quantum systems,” *Europhys. Lett.* **67**, 565 (2004).
- [42] M. Xu, D. A. Tieri, E. C. Fine, J. K. Thompson, and M. J. Holland, “Synchronization of two ensembles of atoms,” *Phys. Rev. Lett.* **113**, 154101 (2014).
- [43] D. Meiser and M. J. Holland, “Intensity fluctuations in steady-state superradiance,” *Phys. Rev. A* **81**, 063827 (2010).
- [44] A. A. Houck, H. E. Treci, and J. Koch, “On-chip quantum simulation with superconducting circuits,” *Nat. Phys.* **8**, 292 (2012).
- [45] Y. Salathé, M. Mondal, M. Oppliger, J. Heinsoo, P. Kurpiers, A. Potočnik, A. Mezzacapo, U. Las Heras, L. Lamata, E. Solano, S. Filipp, and A. Wallraff, “Digital quantum simulation of spin models with circuit quantum electrodynamics,” *Phys. Rev. X* **5**, 021027 (2015).
- [46] C. Müller, J. H. Cole, and J. Lisenfeld, “Towards understanding two-level-systems in amorphous solids: insights from quantum circuits,” *Rep. Prog. Phys.* **82**, 124501 (2019).
- [47] I. Carusotto, A. Houck, A. Kollár, P. Roushan, D. Schuster, and J. Simon, “Photonic materials in circuit quantum electrodynamics,” *Nat. Phys.* , 268 (2020).
- [48] A. Kollár, M. Fitzpatrick, and A. Houck, “Hyperbolic lattices in circuit quantum electrodynamics,” *Nature* **571**, 45 (2019).
- [49] D. Reitz, C. Sayrin, R. Mitsch, P. Schneeweiss, and A. Rauschenbeutel, “Coherence properties of nanofiber-trapped cesium atoms,” *Phys. Rev. Lett.* **110**, 243603 (2013).
- [50] A. Goban, C.-L. Hung, S.-P. Yu, J.D. Hood, J.A. Muniz, J.H. Lee, M.J. Martin, A.C. McClung, K.S. Choi, D.E. Chang, O. Painter, and H.J. Kimble, “Atom-light interactions in photonic crystals,” *Nat. Commun.* **5**, 3808 (2014).
- [51] J. S. Douglas, T. Caneva, and D. E. Chang, “Photon molecules in atomic gases trapped near photonic crystal waveguides,” *Phys. Rev. X* **6**, 031017 (2016).
- [52] H. Bernien, S. Schwartz, A. Keesling, H. Levine, A. Omran, H. Pichler, S. Choi, A. S. Zibrov, M. Endres, M. Greiner, V. Vuletić, and M. D. Lukin, “Probing many-body dynamics on a 51-atom quantum simulator,” *Nature* **551**, 579 (2017).
- [53] R. Yalla, M. Sadgrove, K. P. Nayak, and K. Hakuta, “Cavity quantum electrodynamics on a nanofiber using a composite photonic crystal cavity,” *Phys. Rev. Lett.* **113**, 143601 (2014).
- [54] M. Arcari, I. Söllner, A. Javadi, S. Lindskov Hansen, S. Mahmoodian, J. Liu, H. Thyrrestrup, E. H. Lee, J. D. Song, S. Stobbe, and P. Lodahl, “Near-unity coupling efficiency of a quantum emitter to a photonic crystal waveguide,” *Phys. Rev. Lett.* **113**, 093603 (2014).
- [55] J. T. Barreiro, M. Müller, P. Schindler, D. Nigg, T. Monz, M. Chwalla, M. Hennrich, C. F. Roos, P. Zoller, and R. Blatt, “An open-system quantum simulator with trapped ions,” *Nature* **470**, 486 (2011).
- [56] I. Bloch, J. Dalibard, and W. Zwerger, “Many-body physics with ultracold gases,” *Rev. Mod. Phys.* **80**, 885 (2008).
- [57] I. Bloch, J. Dalibard, and S. Nascimbéne, “Quantum simulations with ultracold quantum gases,” *Nat. Phys.* **8**, 267 (2012).

## Supplemental material: Boosting quantum battery performance by structure engineering

In this supplemental material, we analyze spin dynamics in the single-excitation sector, derive coupled equations of motion for spin operators, which govern the dynamics of quantum battery (QB) in the storage phase while taking into account many-excitation sectors, and present additional simulation results that complement those included in the main text.

### I. DYNAMICAL EVOLUTION IN THE SINGLE-EXCITATION SECTOR

In the main text, we presented simulations for  $\langle \sigma_j^z(t) \rangle$  and  $\langle \sigma_j^+(t) \sigma_{j'}^-(t) \rangle$  based on Eqs. (S8) and (S10) below, respectively. For completeness of our presentation, we cover here essential results from Ref. [40] to explain how these expressions are derived.

In the single-excitation sector, spin dynamics is fully governed by the master equation  $\partial \rho_S / \partial t = \mathcal{K} \rho_S = -i(K \rho_S - \rho_S K^\dagger)$  with  $K = H_S - i \sum_j \frac{\gamma_j}{2} \sigma_j^+ \sigma_j^-$  a quadratic effective Hamiltonian. To solve this master equation, one just needs the eigenspectrum of  $K$ . We place the eigenvalues in the vector  $\Omega = (\{\Omega_n\})$  and organize the right and left eigenvectors of  $K$  in the matrices  $M_R = (\{K_n\})$ ,  $M_L = (\{K_n^*\})$  respectively, with  $n$  running from 1 to  $N$ . Resorting to the Jordan-Wigner transformation tailored for the single-excitation subspace, one finds the following eigenvalues

$$\Omega = (\{\Omega_k^-\}, \{\Omega_k^+\}) = (\Omega_1, \Omega_2, \Omega_3, \dots, \Omega_N), \quad (\text{S1})$$

where  $\Omega_k^\pm$  is given by [40]

$$\Omega_k^\pm = \frac{\Omega_A + \Omega_B}{2} \pm \frac{1}{2} \sqrt{(\Omega_A - \Omega_B)^2 + 16\lambda^2 \cos^2(k/2)}. \quad (\text{S2})$$

$\Omega_{A(B)} = \Delta_{A(B)} - i\gamma_{A(B)}$  and  $k = 2\pi l / (N + 1)$  with  $l = 1, 2, \dots, N/2$ . The eigenvalues of  $K^\dagger$  are the complex conjugates  $\Omega_k^{\pm*}$ .

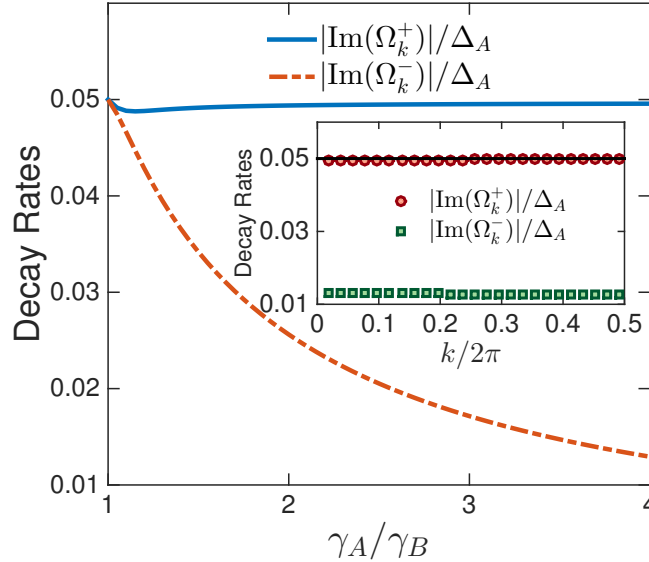


Figure S1. Decay rates  $|\text{Im}(\Omega_k^+)/\Delta_A$  (blue solid line) and  $|\text{Im}(\Omega_k^-)/\Delta_A$  (red dash-dotted line) of the one-excitation sector with varying ratio  $\gamma_A/\gamma_B$  and a fixed  $k = 20\pi/(N + 1)$ . Inset: Decay rates  $|\text{Im}(\Omega_k^+)/\Delta_A$  (red circles) and  $|\text{Im}(\Omega_k^-)/\Delta_A$  (green squares) as a function of index  $k = 2\pi l / (N + 1)$  ( $l = 1, 2, \dots, N/2$ ) with  $\Delta_B = 0.25\Delta_A$ . The black solid line marks the uniform decay rate  $|\text{Im}(\Omega_k^+)| = |\text{Im}(\Omega_k^-)|$  for the uniform lattice with  $\Delta_B = \Delta_A$ . Other parameters are  $N = 50$ ,  $\gamma_j/\Delta_j = 0.05$ ,  $\lambda = 0.05\Delta_A$ .

In general, the eigenvalues of the Liouvillian  $\mathbb{L}$  can be constructed by using  $\Omega_k^\pm$  and  $\Omega_k^{\pm*}$  as detailed in Ref. [39]. Interestingly, for the single-excitation sector with smallest decay rates, the corresponding eigenvalues of the Liouvillian  $\mathbb{L}$  are  $-i\Omega_k^\pm$  and  $i\Omega_k^{\pm*}$ . Hence, the absolute values of the imaginary parts of  $\Omega_k^\pm$  set the decay rates of the slowest modes. As can be seen, for uniform

spin lattice with  $\gamma_A = \gamma_B \equiv \gamma_0$ , we get  $\Omega_A = \Omega_B$ , hence the imaginary parts of  $\Omega_k^\pm$  coincide, and take the value  $\gamma_0$ ; for uniform QBs,  $\gamma_0^{-1}$  sets the storage time scale [12]. In contrast, for dimeric lattices with  $\gamma_A \neq \gamma_B$ , the intrinsic decay rates are modified. Noting that for vanishing dipole-dipole interactions,  $\lambda = 0$ , we still have two bands provided that  $\Omega_A \neq \Omega_B$ . In Fig. S1, we present results for the decay rates  $|\text{Im}(\Omega_k^\pm)|$  ('Im' takes imaginary part hereafter) for the slowest single-excitation sector. From Fig. S1 and its inset, we clearly observe that the engineered decay rates  $|\text{Im}(\Omega_k^\pm)|$  of two bands in dimeric spin lattices can be made both smaller than that of the uniform limit ( $\gamma_A = \gamma_B = 0.05\Delta_A$  in present simulations), thereby implying a much longer storage time for a dimeric QB, as compared with its non-engineered counterpart.

The corresponding eigenvectors are expressed as [40]

$$\mathbf{M}_R = (\{v'_k|g\rangle\}, \{u'_k|g\rangle\}), \quad \mathbf{M}_L = (\{|g\rangle v_k\}, \{|g\rangle u_k\}). \quad (\text{S3})$$

Here,  $|g\rangle$  is the global ground state of the spin lattice with  $\sigma_j^z|g\rangle = -|g\rangle$ . The operators  $u'_k, v'_k$  are defined as

$$\begin{aligned} v'_k &= \sqrt{\frac{4}{N+1}} \sum_{m=1}^{N/2} (\sigma_{2m-1}^+ \sin \theta_k \sin[k(m-1/2)] + \sigma_{2m}^+ \cos \theta_k \sin(km)), \\ u'_k &= \sqrt{\frac{4}{N+1}} \sum_{m=1}^{N/2} (\sigma_{2m-1}^+ \cos \theta_k \sin[k(m-1/2)] - \sigma_{2m}^+ \sin \theta_k \sin(km)). \end{aligned} \quad (\text{S4})$$

Here,  $\theta_k$  is determined by  $\tan 2\theta_k = -4\lambda \cos(k/2)/(\Delta_A - \Delta_B - i(\gamma_A - \gamma_B))$ . Operators  $v_k$  and  $u_k$  are obtained from  $v'_k$  and  $u'_k$ , by replacing spin raising operators with lowering ones, respectively.

In terms of the eigenvectors of the effective Hamiltonian  $K$ , we introduce the decomposition of the reduced system density matrix

$$\rho_S = \left( \sum_{nm} \mathcal{P}_{n,m} + \sum_n \mathcal{P}_{n,0} + \sum_n \mathcal{P}_{0,n} + \mathcal{P}_{0,0} \right) \rho_S. \quad (\text{S5})$$

Here,  $n, m$  are indices running from 1 to  $N$ , we denote projectors as

$$\begin{aligned} \mathcal{P}_{n,m}\rho_S &= \langle K_n^* | \rho_S | K_m^* \rangle |K_n\rangle \langle K_m|, \\ \mathcal{P}_{n,0}\rho_S &= \langle K_n^* | \rho_S | g \rangle |K_n\rangle \langle g|, \\ \mathcal{P}_{0,n}\rho_S &= \langle g | \rho_S | K_n^* \rangle |g\rangle \langle K_n|, \\ \mathcal{P}_{0,0}\rho_S &= \langle g | \rho_S | g \rangle |g\rangle \langle g|. \end{aligned} \quad (\text{S6})$$

To illustrate the occurrence of quantum synchronization, we study the ensemble average  $\langle \sigma_j^x(t) \rangle$ ,

$$\begin{aligned} \langle \sigma_j^x(t) \rangle &= 2\text{Re}\langle \sigma_j^-(t) \rangle = 2\text{Re}\langle e_j | \rho_S(t) | g \rangle \\ &= 2\text{Re}\langle e_j | \sum_n \mathcal{P}_{n,0} \rho_S(t) | g \rangle. \end{aligned} \quad (\text{S7})$$

Here,  $|e_j\rangle = \sigma_j^+ |g\rangle$ . It is easy to show that  $\mathcal{P}_{n,0}\rho_S(t) = \mathcal{P}_{n,0}\rho_S(0)e^{-i\Omega_n t}$  using  $\mathcal{K}|K_n\rangle \langle g| = -i\Omega_n |K_n\rangle \langle g|$ , hence we have

$$\langle \sigma_j^x(t) \rangle = 2\text{Re} \left[ \sum_{n=1}^N F_n(j) e^{-i\Omega_n t} \right], \quad (\text{S8})$$

with  $F_n(j) = \langle K_n^* | \rho_S(0) | g \rangle \langle e_j | K_n \rangle$  and  $\rho_S(0) = |\Phi_0\rangle \langle \Phi_0|$  ( $|\Phi_0\rangle$  is the initial state). For our purpose, we also consider  $\langle \sigma_j^z(t) \rangle$  in the single-excitation sector. Using Eq. (S5) and the relation  $\mathcal{P}_{n,m}\rho_S(t) = \mathcal{P}_{n,m}\rho_S(0)e^{-i(\Omega_n - \Omega_m^*)t}$ , we immediately find that

$$\langle \sigma_j^z(t) \rangle = 2\langle e_j | \sum_{n,m} \mathcal{P}_{n,m}\rho_S(t) | e_j \rangle - 1 = 2 \sum_{n=1, m=1}^N G_{n,m}(j) e^{-i(\Omega_n - \Omega_m^*)t} - 1. \quad (\text{S9})$$

Here,  $G_{n,m}(j) = \langle e_j | K_n \rangle \langle K_m | e_j \rangle \langle K_n^* | \rho_S(0) | K_m^* \rangle$  with  $|K_n^*\rangle$  and  $\langle K_n|$  the right and left eigenvectors of  $K^\dagger$  with eigenvalues  $\Omega_n^*$ . Analogously, we obtain the following expression for spin-spin correlations  $\langle \sigma_j^+(t) \sigma_{j'}^-(t) \rangle$ :

$$\begin{aligned} \langle \sigma_j^+(t) \sigma_{j'}^-(t) \rangle &= \langle e_{j'} | \rho_S(t) | e_j \rangle \\ &= \sum_{n=1, m=1}^N W_{n,m}(j, j') e^{-i(\Omega_n - \Omega_m^*)t} \end{aligned} \quad (\text{S10})$$

with  $W_{n,m}(j, j') = \langle K_n^* | \rho_S(0) | K_m^* \rangle \langle K_m | e_{j'} \rangle \langle e_j | K_n \rangle$ .

In Fig. S2, we present trajectories  $\langle \sigma_j^x(t) \rangle$  using Eq. (S8) while varying the frequency ratio  $\Delta_B/\Delta_A$ . From this comparison, we observe that for relative small ratios  $\Delta_B/\Delta_A$  a phase synchronization emerges at the trajectory level as the two trajectories depict almost perfect anti-phase oscillations, while when the ratio  $\Delta_B/\Delta_A$  approaches unity, this anti-phase oscillation becomes obscure as can be seen from Fig. S2 (d), consistent with findings in Ref. [40] for short lattices.

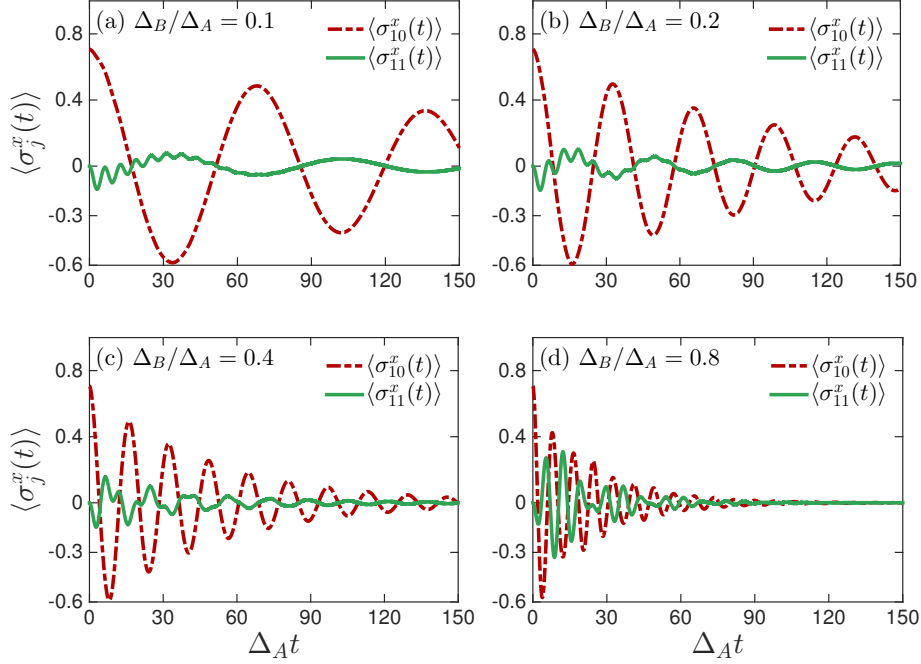


Figure S2. Trajectories for  $\langle \sigma_{10}^x(t) \rangle$  (red dash-dotted line) and  $\langle \sigma_{11}^x(t) \rangle$  (green solid line) using Eq. (S8) for a dimeric lattice while varying the detuning ratio  $\Delta_B/\Delta_A$ . (a)  $\Delta_B/\Delta_A = 0.1$ , (b)  $\Delta_B/\Delta_A = 0.2$ , (c)  $\Delta_B/\Delta_A = 0.4$ , and (d)  $\Delta_B/\Delta_A = 0.8$ . We adopt the initial state  $|g\rangle/\sqrt{2} + (|e_{j=10}\rangle + |e_{j=12}\rangle)/2$ . Other parameters are  $N = 50$ ,  $\gamma_j/\Delta_j = 0.05$ ,  $\lambda = 0.05\Delta_A$ .

## II. MANY EXCITATIONS CASE: DYNAMICAL EQUATIONS FOR EXPECTATION VALUES OF SPIN OPERATORS

In this section, we first illustrate how to introduce a superradiant decay channel for spins in the discharging phase when the cavity is coupled to the spin chain. To this end, we consider the so-called bad cavity limit,  $\kappa \gg \eta$ ,  $\gamma_j$  [12]. In this limit, the cavity degrees of freedom can be adiabatically eliminated using the solution [42]

$$a \simeq -\frac{2i\eta}{\kappa + i\Delta_A} J_A^- - \frac{2i\eta}{\kappa + i\Delta_B} J_B^-, \quad (\text{S11})$$

where  $J_{A(B)}^- \equiv \sum_{j \in \text{odd(even)}} \sigma_j^-$  are collective lowering spin operators. Noting that frequency detuning  $\Delta_{A,B} = \omega_{A,B} - \omega_c$  can be made small relative to  $\kappa$  for bad cavities, we simplify Eq. (S11) as  $a \simeq -2i\eta J^- / \kappa$  with  $J^- = J_A^- + J_B^- = \sum_j \sigma_j^-$ , yielding

$$\frac{\partial}{\partial t} \rho_S = -i[H_S, \rho_S] + \sum_{j=1}^N \gamma_j \mathcal{L}[\sigma_j^-] \rho_S + \Gamma \mathcal{L}[J^-] \rho_S. \quad (\text{S12})$$

Here,  $H_S = \sum_{j=1}^N \frac{\Delta_j}{2} \sigma_j^z + \sum_{j=1}^{N-1} \lambda (\sigma_j^+ \sigma_{j+1}^- + \text{H.c.})$  is the Hamiltonian of dimer spin lattice,  $\Gamma = 4\eta^2/\kappa$  denotes a Purcell-enhanced emission rate marking a cavity-induced superradiant process, which is designed to be the dominant decay channel for spins in the discharging phase. By setting  $\Gamma = 0$ , we recover the quantum master equation used for analyzing the storage phase in the main text.

To derive dynamical equations from the master equation Eq. (S12), we use the relations  $\text{Tr}\{A[H_S, \rho_S]\} = \text{Tr}\{[A, H_S]\rho_S\}$  and

$$\text{Tr}\{A\mathcal{L}[O]\rho_S\} = \frac{1}{2}\text{Tr}\{[O^\dagger, A]O\rho_S\} + \frac{1}{2}\text{Tr}\{\rho_S O^\dagger[A, O]\} \quad (\text{S13})$$

for an arbitrary spin operator  $A$  and a Lindblad superoperator  $\mathcal{L}[O]\rho_S = (2O\rho_S O^\dagger - O^\dagger O\rho_S - \rho_S O^\dagger O)/2$ . The dynamical equation for  $\langle \sigma_j^z \rangle$  takes the form (explicit time dependence is suppressed hereafter):

$$\begin{aligned} \frac{d}{dt} \langle \sigma_j^z \rangle = & -2i\lambda [\langle \sigma_j^+ \sigma_{j+1}^- \rangle + \langle \sigma_j^+ \sigma_{j-1}^- \rangle - \langle \sigma_{j+1}^+ \sigma_j^- \rangle - \langle \sigma_{j-1}^+ \sigma_j^- \rangle] - \gamma_j (1 + \sigma_j^z) \\ & - \Gamma (1 + \sigma_j^z) - \Gamma \sum_{m \neq j} [\langle \sigma_j^+ \sigma_m^- \rangle + \text{c.c.}], \end{aligned} \quad (\text{S14})$$

where ‘c.c.’ denotes complex conjugate. From the above equation of motion, it is evident that the discharging phase always benefits from a superradiant decay channel with a Purcell-enhanced emission rate,  $\Gamma \gg \gamma_{A,B}$ , thereby achieving a fast discharging process [12]. We highlight that our setup lacks a permutation symmetry, that is, spin correlations depend on the indices due to the presence of a nearest-neighbor dipole-dipole coupling, in contrast to the scenario studied in Ref. [12].

The above dynamical equation should be solved subject to those for  $\langle \sigma_n^+ \sigma_m^- \rangle$ . Below we limit our attention to the storage phase when  $\Gamma$  is tuned to zero. For  $\langle \sigma_n^+ \sigma_m^- \rangle$ , we find it convenient to separately treat two scenarios, due to the presence of nearest-neighbor dipole-dipole coupling: (i)  $m = n \pm 1$  and (ii)  $m \neq n, n \pm 1$ ,

- Case (i):

$$\begin{aligned} \frac{d}{dt} \langle \sigma_n^+ \sigma_{n\pm 1}^- \rangle &= \left[ i(\Delta_n - \Delta_{n\pm 1}) - \frac{\gamma_n + \gamma_{n\pm 1}}{2} \right] \langle \sigma_n^+ \sigma_{n\pm 1}^- \rangle \\ &\quad - i\frac{\lambda}{2} [\langle \sigma_n^z \rangle - \langle \sigma_{n\pm 1}^z \rangle] - i\lambda [\langle \sigma_n^z \sigma_{n\mp 1}^+ \sigma_{n\pm 1}^- \rangle - \langle \sigma_{n\pm 1}^z \sigma_n^+ \sigma_{n\pm 2}^- \rangle]. \end{aligned} \quad (\text{S15})$$

- Case (ii):

$$\begin{aligned} \frac{d}{dt} \langle \sigma_n^+ \sigma_m^- \rangle &= \left[ i(\Delta_n - \Delta_m) - \frac{\gamma_n + \gamma_m}{2} \right] \langle \sigma_n^+ \sigma_m^- \rangle \\ &\quad - i\lambda \sum_{h=n\pm 1} \langle \sigma_n^z \sigma_m^- \sigma_h^+ \rangle + i\lambda \sum_{h=m\pm 1} \langle \sigma_m^z \sigma_n^+ \sigma_h^- \rangle. \end{aligned} \quad (\text{S16})$$

To form a closed set of coupled dynamical equations, we adopt a semiclassical cumulant approximation that is applicable to large spin numbers: correlations are expanded to second order. Particularly, here we approximate  $\langle \sigma_n^z \sigma_m^+ \sigma_h^- \rangle \approx \langle \sigma_n^z \rangle \langle \sigma_m^+ \sigma_h^- \rangle$  [43]. By doing so, we neglect correlations of the type  $\langle \sigma_n^z \sigma_m^+ \rangle$  ( $n \neq m$ ) [42]. Accordingly, we approximate Eqs. (S15) and (S16) as

- Case (i):

$$\begin{aligned} \frac{d}{dt} \langle \sigma_n^+ \sigma_{n\pm 1}^- \rangle &\approx \left[ i(\Delta_n - \Delta_{n\pm 1}) - \frac{\gamma_n + \gamma_{n\pm 1}}{2} \right] \langle \sigma_n^+ \sigma_{n\pm 1}^- \rangle - i\frac{\lambda}{2} [\langle \sigma_n^z \rangle - \langle \sigma_{n\pm 1}^z \rangle] \\ &\quad - i\lambda [\langle \sigma_n^z \rangle \langle \sigma_{n\mp 1}^+ \sigma_{n\pm 1}^- \rangle - \langle \sigma_{n\pm 1}^z \rangle \langle \sigma_n^+ \sigma_{n\pm 2}^- \rangle]. \end{aligned} \quad (\text{S17})$$

- Case (ii):

$$\begin{aligned} \frac{d}{dt} \langle \sigma_n^+ \sigma_m^- \rangle &\approx \left[ i(\Delta_n - \Delta_m) - \frac{\gamma_n + \gamma_m}{2} \right] \langle \sigma_n^+ \sigma_m^- \rangle \\ &\quad - i\lambda \sum_{h=n\pm 1} \langle \sigma_n^z \rangle \langle \sigma_h^+ \sigma_m^- \rangle + i\lambda \sum_{h=m\pm 1} \langle \sigma_m^z \rangle \langle \sigma_n^+ \sigma_h^- \rangle. \end{aligned} \quad (\text{S18})$$

Eqs. (S14), (S17) and (S18) form a closed set, which can be numerically propagated by means of, for instance, Runge-Kutta algorithm subject to the open boundary condition for the spin lattice.

### III. ADDITIONAL SIMULATION RESULTS

In this section, we include additional simulations that complement those shown in the main text. For characterizing the performance of QBs in the storage phase, one can also look at the normalized population defined as

$$\mathcal{P}(t) = \frac{\sum_{j=1}^N \frac{\Delta_j}{2} \langle \sigma_j^z(t) \rangle}{\sum_{j=1}^N \Delta_j / 2}. \quad (\text{S19})$$

Similarly to the main text, we denote by  $\mathcal{P}_{d(u)}(t)$  the population of the dimeric (uniform) spin lattice. A typical set of results is presented in Fig. S3. As can be seen, the normalized population depicts almost the same behavior as the normalized energy shown in the main text. Therefore, the normalized population can also serve as a figure of merit for characterizing QBs in the storage phase.

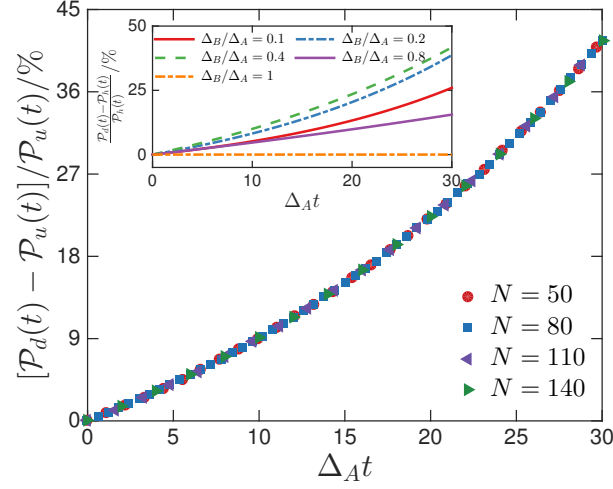


Figure S3. Dynamics of relative excess population  $[\mathcal{P}_d(t) - \mathcal{P}_u(t)]/\mathcal{P}_u(t)$  in the storage phase as a function of spin number  $N$  with a fixed detuning ratio  $\Delta_B/\Delta_A = 0.25$ . The inset shows the relative excess energy when varying the detuning ratio  $\Delta_B/\Delta_A$  and a fixed number of spins  $N = 80$ . Other parameters are  $\gamma_{A(B)}/\Delta_{A(B)} = 0.05$  and  $\lambda = 0.05\Delta_A$ .

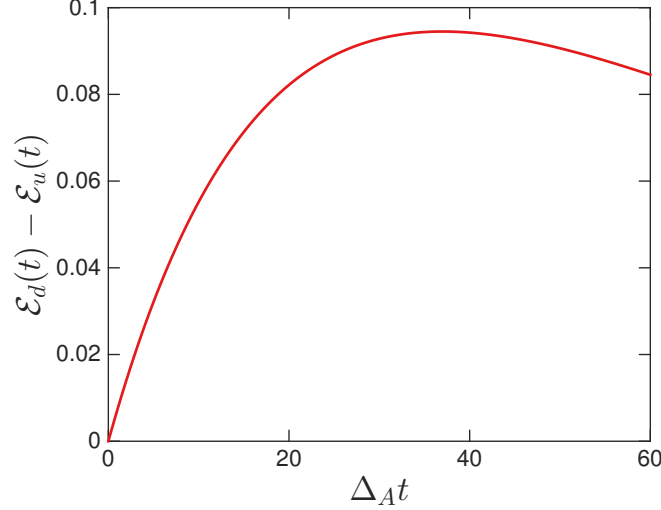


Figure S4. Dynamics of excess energy density  $\mathcal{E}_d(t) - \mathcal{E}_u(t)$  in the storage phase for a dimeric battery with  $\Delta_B/\Delta_A = 0.25$ . Other parameters are  $N = 80$ ,  $\gamma_j/\Delta_j = 0.05$ ,  $\lambda = 0.05\Delta_A$ .

In Fig. S4, we check the long time behavior of the absolute excess energy  $\mathcal{E}_d(t) - \mathcal{E}_u(t)$ . We find that  $\mathcal{E}_d(t) - \mathcal{E}_u(t)$  depicts a turnover behavior when increasing the storage time, indicating that there is an optimal protection time for engineered QBs.

In Fig. S5, we analyze the dependence of  $[\mathcal{E}_d(t) - \mathcal{E}_u(t)]/\mathcal{E}_u(t)$  on time. We observe a power-law behavior,  $\mathcal{E}_d(t)/\mathcal{E}_u(t) \propto t^\alpha$ , with  $\alpha = 1.5$  at longer times.

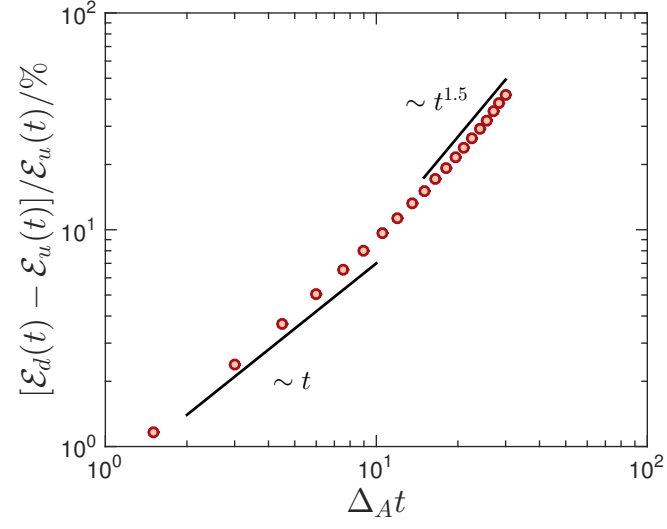


Figure S5. Dynamics of the relative stored energy excess  $[\mathcal{E}_d(t) - \mathcal{E}_u(t)]/\mathcal{E}_u(t)$  as a function of time with a fixed detuning ratio  $\Delta_B/\Delta_A = 0.25$ . Other parameters are  $N = 80$ ,  $\gamma_{A(B)}/\Delta_{A(B)} = 0.05$  and  $\lambda = 0.05\Delta_A$ .